Int. J. Electrochem. Sci., 16 **(2021)** 210259, doi: 10.20964/2020.08.89

International Journal of
ELECTROCHEMICAL
SCIENCE
www.electrochemsci.org

Short Communication

Ag-doped ZnO nanorods synthesized on Porous Si electrode using a facile electrochemical approach for Removal of Methylene Blue from wastewater

Ye Yu

School of landscape architecture, Beijing Forestry University, Beijing 100083, China
E-mail: yeyuyy66@163.com, ye_yu@bjfu.edu.cn

Received: 4 April 2020 / *Accepted:* 1 June 2020 / *Published:* 31 December 2020

The enhanced photocatalytic features of the synthesized materials indicates their potentiality in wastewater treatment. In this work, vertically aligned silver (Ag) doped-ZnO nanorods (NRs) were successfully synthesized on seed-layer-free PSi structures using an electrochemical technique and FESEM results indicated that c-axis orientation was the preferential growth direction of the single-crystalline Ag doped-ZnO NRs, consistent with XRD results. Electrochemical impedance spectroscopy (EIS) was applied to analyze the interface properties and charge transfer efficiency of samples. The removal of methylene blue as an organic compound in wastewater using the Ag doped-ZnO/PSi photoanodes was studied by the photoelectrocatalytic technique. The EIS results showed that Ag doped-ZnO/PSi nanostructures have higher free-electron carriers which accelerate charge transfer and decrease the resistance. The enhanced photocatalytic activity of the Ag doped-ZnO/PSi can be attributed to the enhancement of photogenerated electron-hole pairs as a result of varied potential energy between ZnO and Ag.

Keywords: Ag doped-ZnO/PSi nanostructures; Electrochemical technique; Photoelectrocatalytic; Wastewater; Methylene blue

1. INTRODUCTION

Recently, the development of innovative techniques for wastewater and water treatment and management has attracted the attention of many scientific activities and research projects [1, 2]. Common methods used to treat wastewater frequently fail to completely degrade toxic compounds, or yield large amounts of waste activated sludge, which can cause defecation problems [3]. An environmental favorable alternative is offered by advanced oxidation procedures [4]. Among them, semiconductor-based photocatalytic degradation, which uses metal oxide materials as a catalyst to act as an oxidation medium, is widely used [5].

Zinc oxide (ZnO) is eliciting research interest due to the large exciton binding energy of 60 meV, its wide band gap, and stable physical and chemical properties [6]. Accordingly, ZnO-based nanostructures such as nanorods (NRs) or nanowires are considered as promising materials for various wide-ranging applications such as in the field of photocatalysis and sensing. Porous Si (PSi) structures are commonly have surfaces morphology that are rough which are the best templates for the growth of align ZnO nanostructures with minimal stress and without metal catalysts [7].

ZnO nanostructures have been produced using a variety of methods [8]. Among them, the electro-electrochemical technique is the most commonly used for its safety, simplicity, and low-temperature deposition.

The localization and transport processes of charge mainly assess the functional properties of film-based photoelectrodes [9]. The surface environmental composition is one of the important factors in the fluctuation of electrical properties of the layers. Notably, metal oxides nanocomposites consist of regions with distinct electrical properties [10]. The photocatalytic efficiency can be affected by a disadvantage of ZnO, the rapid recombination of photoexcited hole and electron pairs. To overcome this disadvantage, the recombination rate of the pair must be slowed down and the surface charge transfer must be improved. A number of methods have been devised to alter these and one of them is doping the ZnO photocatalysts with a transition metal, which can result in alteration of electrical, magnetic and optic properties of ZnO [11]. It also results in a decrease of band gap energy, the formation of electron traps to increase the charge separation and better photo catalysis activity of ZnO. Doping of ZnO is widely done by using transition metals such as Ni, Mn, Fe, Cu, and Ag [12-14]. This enables the formation of electron traps that decrease the pair recombination rate. It has been found that doping is an effective process in the photocatalytic activities only when added in optimum concentration.

Electrochemical impedance spectroscopy (EIS) is widely used to study various other electrochemical systems such as corrosion, electrodeposition, batteries, and fuel cells. However, impedance techniques have recently been used in the photocatalytic field.

In the present study, a new approach was established to investigate Ag doped-ZnO/PSi photoelectrode through an EIS technique. The photocatalytic efficiency of the obtained Ag doped-ZnO NRs were intensely considered for the possible approach in water treatment.

2. MATERIALS AND METHODS

The n-type PSi structure was made on Si (100) oriented wafer using a photoelectrochemical wet etching process in a home-made Teflon cell. This cell contains a mixture of ethanol (96%) and hydrofluoric acid (HCl) with a 4:1 volume ratio. Prior to etching, the samples were cleaned using the standard RCA procedure and dried by blowing nitrogen. The platinum wire as a cathode and the Si sample as an anode were connected to a direct external power supply. Etching time and current density were 8 min and 20 mA/cm^2, respectively which were utilized to prepare a PSi layer. Ag doped- ZnO NRs were prepared by electrochemical technique on PSi substrates. A two-electrode setup was used to deposit Ag doped-ZnO NRs on PSi substrates. 0.1M zinc nitrate hexahydrate ($Zn(NO_3)_2.6H_2O$) and

0.05M silver nitrate ($AgNO_3$) were added to DI water and subjected to 30 min vigorous stirring. 0.1M hexamethylenetetramine (HMTA) was dissolved in 25 ml DI water and then was added to the previous solution. After stirring and uniform mixing, a few drops of ammonium hydroxide (NH_4OH) were added to adjust the pH to 10. A homogenous mixture was made by stirring it for 20 min. The 25 mM aqueous solution was put into a galvanic cell. The PSi and Pt electrodes were exposed to the solution as the cathode and anode, respectively. Vertically aligned nano tapered ZnO structures were produced with 1 mA/cm^2 current density, 60 min growth time and 80 °C growth temperature.

FEI/Nova NanoSEM 450 Field-emission scanning electron microscopy (FESEM) was used to characterize structure, morphology and size of the Ag doped- ZnO NRs. X-ray diffraction (XRD; PANalytical X'Pert PRO MRD PW3040) was employed to evaluate the crystallinity Ag doped- ZnO NRs/PSi nanostructures.

Electrochemical impedance spectroscopy (EIS) was used to examine the charge transfer and recombination processes with a 10 mV potential at frequencies range from 0.1 Hz to 0.1MHz. In typical measurement, Ag-doped ZnO nanorods grown on PSi substrates were used as the working electrode. An Ag/AgCl and Pt wire were utilized as the reference and counter electrodes, respectively. 0.1M sodium sulfate (Na_2SO_4) aqueous solution was used as the electrolyte in this experiment. The photoelectrocatalytic of the Ag doped- ZnO NRs/PSi electrode was investigated by degradation of MB dye under UV irradiation. The photoelectron-degradation tests were performed in an electrochemical cell, including of three electrodes. Ag doped- ZnO NRs/Psi, Pt mesh electrode and Ag/AgCl/KCl, as working, counter and reference electrodes, respectively. The cell was filled by 25 mg L^{-1} of MB aqueous solution in 400 mL Na_2SO_4. A positive potential of 0.6 V was used for a period of 2 hours.

Tap-water and wastewater were used as real samples in this study. Wastewater with COD between 400 and 600 mg/L was obtained from a chemical products factory in Beijing, China. pH meter (Sigma, P1367 MSDS) was applied for adjusting the pH of solutions. The real samples after separation were analysed to determine the residual MB concentration by UV spectrophotometer at 665 nm. The extent of dye removal expressed as percentage was calculated using the following equation:

$$\text{Removal efficiency (\%)} = [(C_0 - C_r)/C_0] \times 100 \quad (1)$$

where C_0 and C_r is the initial and residual concentrations of MB in solution (mg/L), respectively.

3. RESULTS AND DISCUSSION

The FESEM image in Figure 1a shows high-density Ag doped- ZnO NRs uniformly distributed over the whole PSi substrate. Figure 1b demonstrates well-aligned and perpendicular Ag doped-ZnO NRs on the naked PSi surface as approved by the (002) peaks discovered in the XRD patterns. The figure indicates that a sponge-like structure was formed at the Si surface with a lot of pores. The pore sizes were between 15 and 50 nm and are shown by black areas in the image. The average surface roughness of the pores was 2.124 nm, whereas that of silicon wafer was 0.314 nm. The rough surface of PSi provided suitable planes for the Ag doped-ZnO nanostructures. The heterogeneous surface textures helped Ag doped-ZnO nanostructures to grow with minimal lattice mismatch and stress.

Furthermore, the presence of a PSi layer prepared an alternative energy pathway and reduced the activation energy for the growth and nucleation of Ag doped-ZnO nanostructures.

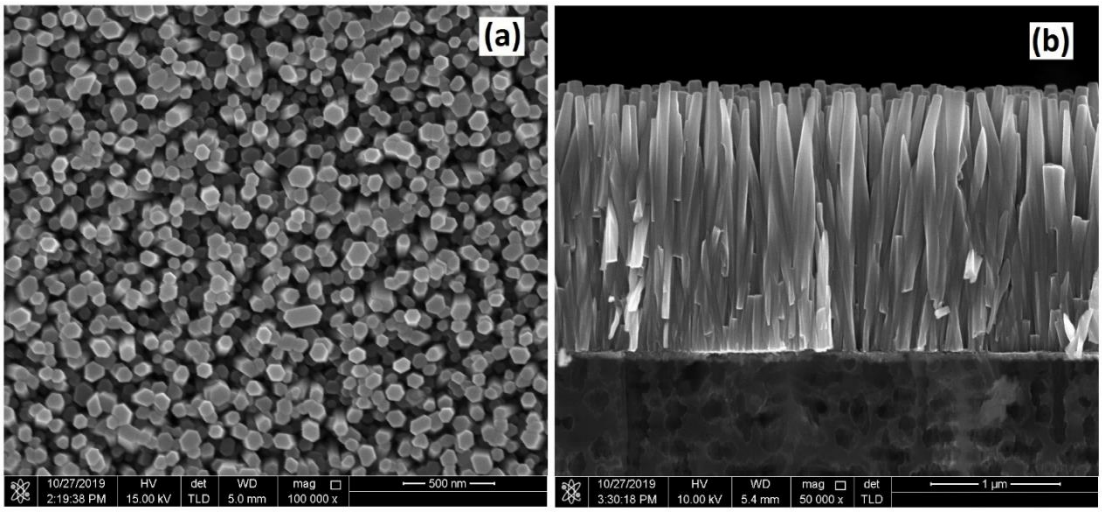

Figure 1. FESEM images of (a) surface, (b) cross-sectional Ag doped-ZnO/Psi synthesized at 1 mA/cm^2 current density, 60 min growth time and 80 °C growth temperature.

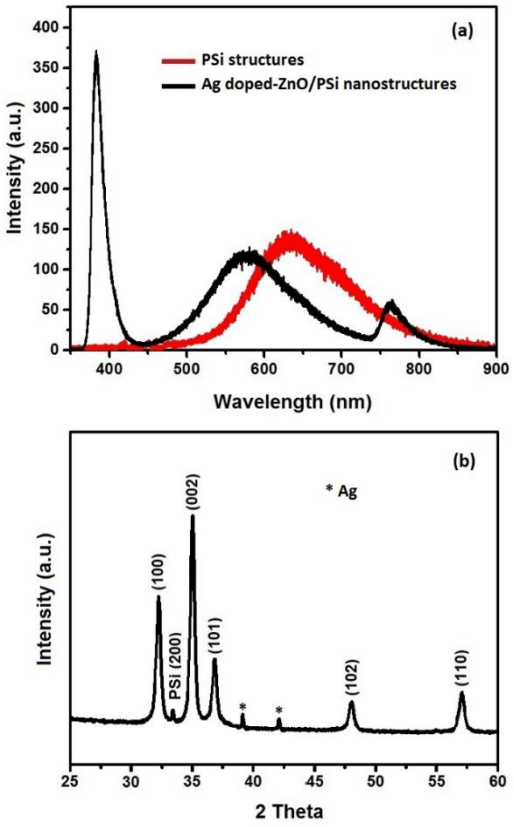

Figure 2. (a) PL spectra of the bare PSi and Ag doped-ZnO/PSi nanostructures (b) XRD pattern of Ag doped-ZnO/PSi nanostructures synthesized at 1 mA/cm^2 current density, 60 min growth time and 80 °C growth temperature.

Figure 2a exhibits the PL spectrum of PSi and Ag doped-ZnO NR arrays grown on PSi substrate. PSi indicated a high intensity peak in 637.4 nm, representing the superior quality of PSi substrate [15]. The strong and sharp luminescence peak at 379.82 nm corresponded to the excitonic recombination related to the near-band edge emission [16].

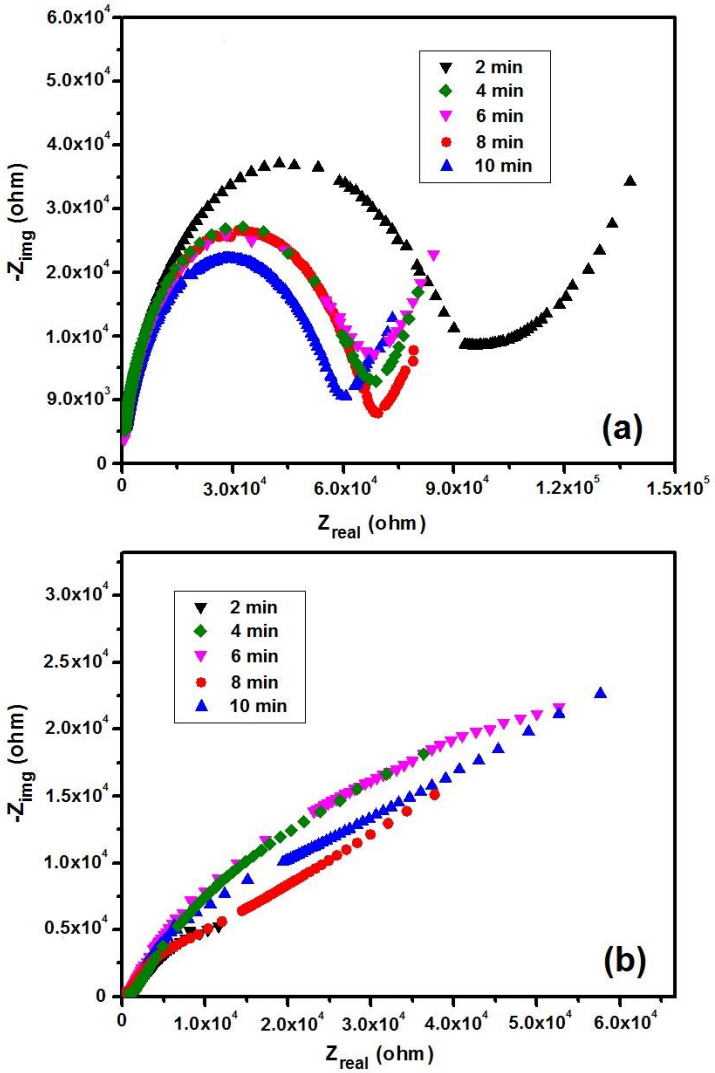

Figure 3. Nyquist diagrams of (a) Porous Si and (b) Ag doped-ZnO/Psi electrodes after exposure to 0.1M Na_2SO_4 solution with a potential of 10 mV.

The visible-range emission of Ag doped-ZnO NRs (500–700 nm) can be associated to radiative recombination through intrinsic defects and structural in the ZnO lattice structure, such as zinc vacancies, oxygen vacancies, zinc interstitials, oxygen interstitials, and antisite defects that formed deep energy levels within the band gap of Ag doped-ZnO. The presence of a small emission peak at 762 nm may be attributed to the 2nd order diffraction spectrum of high-intensity UV light [17].

The XRD patterns of Ag doped-ZnO/PSi NR structures were evaluated to consider their structural properties (Figure 2b). The XRD diffraction peaks suggested a polycrystalline nature. The narrower and higher intensity of the (002) diffraction peak indicated the preferred ZnO NRs growth

[18], which moved to the *c*-axis; this finding can be related to the low interfacial free energy of the (002) lattice plane. Three additional peaks appeared at 38.1 and 44.2 which can be associated to (111) and (200) planes of Ag corresponding to the Ag face-centered cubic (JCPDS file no. 04-0783). The increase of Ag diffraction peaks in XRD pattern obviously confirmed the Ag doping in ZnO nanostructures.

The interface properties and charge transfer efficiency of samples had been investigated by electrochemical impedance measurement [19]. The Nyquist diagrams of PSi and Ag doped-ZnO/PSi nanostructures for 10 min exposed time to 0.1 M Na_2SO_4 electrolyte solution are revealed in Figure 3. The changes in real impedance at high and low frequencies was investigated by the resistance of polarization (R_p) with charge-transfer resistance in the low frequency and bulk resistance in the high frequency [20]. PSi substrate showed variations in real impedance and imaginary values after exposure to Na_2SO_4 solution. Once the PSi nanostructure surface was completely covered, chemical molecules diffused among these pores and interacted by the Si surface. As shown in Figure 3a, the semicircle diameter increased significantly in the presence of inhibitor in comparison to those with less exposure time, demonstrating full coating of the film surface with the solution. Two semicircles created for 10 min with increased R_p value of PSi were attained with increased exposure time.

Figure 3b shows the complex Nyquist plot of the Ag doped-ZnO/PSi electrode. The semicircle diameter increased with prolonged exposure time to Na_2SO_4 solution. A straight line could be observed at low frequencies after 4 min for Ag doped-ZnO/PSi nanostructures. Resistance of diffused layer can be recognized as a mechanism of ion diffusion [21]. It appeared after 4 min because Na_2SO_4 solution passed using the ZnO NRs and reached the PSi surface. C_{dl}, R_{ct}, and Warburg impedance were almost constant after an 8 min exposure.

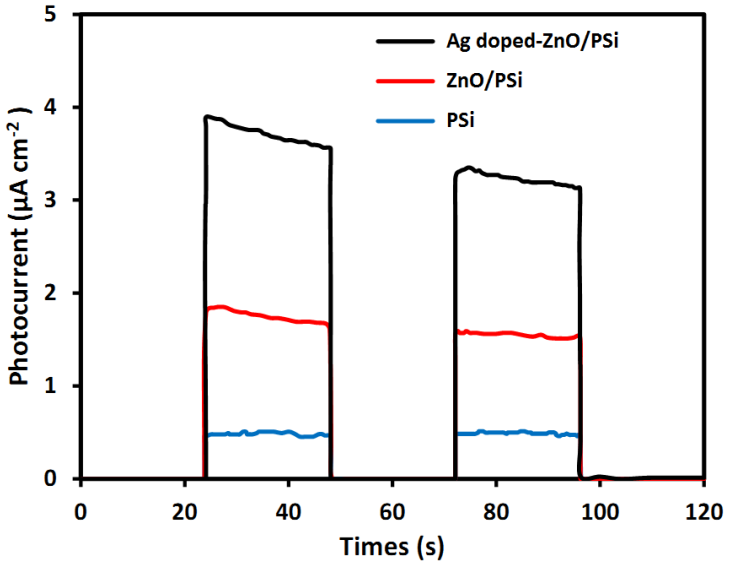

Figure 4. Photocurrent measurements of PSi, ZnO/PSi and Ag doped-ZnO/PSi electrodes in 0.1M Na2SO4 solution

As shown in Figure 3b, a noticeable reduction in the polarization resistance of Ag doped-ZnO/PSi films was gained. The Nyquist diagram of the inhibited solution indicated that the semicircle was not absolutely formed after exposure. The perfectly straight line appeared at exposure time more than 8 min, showing that mass transport was limited by the accumulated species and surface inhibitor film at an exposure time of 8 min. These findings demonstrate that Ag doped-ZnO nanostructures have higher free-electron carriers which accelerate charge transfer and decrease the resistance, it is useful for the enhancement of the ZnO photocatalytic activity.

In order to characterize the different samples' ability of separating of photo-generated electrons and producing charge carriers, the photocurrent measurements were used. As shown in Figure 4, Ag doped-ZnO/PSi shows the strongest photocurrent intensity than PSi and ZnO/Psi electrodes. Therefore, the results imply that Ag doped-ZnO/PSi has better structure and tends to easier produce charge carriers and separated electrons. Because the presence of photo-generated electrons is the key factor in actual photocatalytic performance, Ag doping in ZnO NRs can transfer more photo-generated electrons to protons to improve hydrogen evolution reaction. Thus Ag doped ZnO NRs are expected to exhibit enhanced photocatalytic activity.

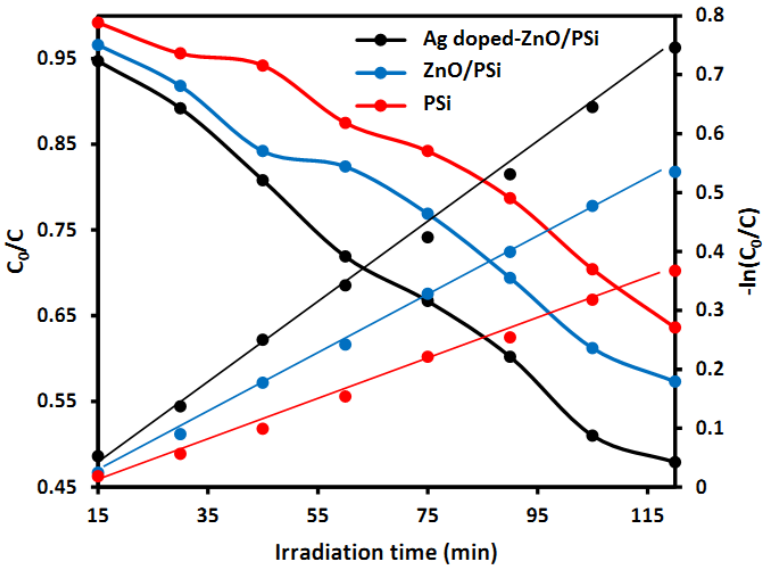

Figure 5. Photodegradation rate of MB dye under UV light irradiation in PSi, ZnO/PSi and Ag doped-ZnO/PSi electrodes at a positive potential of 0.6 V for a period of 2 hours

The photoelectrocatalytic degradation of MB dye under UV-light irradiation was employed to investigate the water treatment activities of PSi, ZnO/PSi and Ag doped-ZnO/PSi electrodes. The photodegradation results of the samples are shown in Figure 5. About 41% of MB was removed in 120 min when the ZnO/PSi photoelectrode was applied for the photoelectrocatalytic process, while it enhanced to 52% when using the Ag doped-ZnO/PSi electrode. Fragala et al. [22] prepared ZnO NRs on Si substrate by chemical bath deposition and evaluated the photocatalytic efficiency of the photoelectrode for the degradation of MB. The authors obtained 56% MB removal after 4 hours of treatment. This work indicates that our findings are comparable with those results in the literature for related morphology of ZnO nanomaterials.

Table 1. Overview of the different transition metals-doped ZnO nanostructures with their synthesis techniques and photocatalytic performances.

Doping materials	Synthesis technique	Pollutant	Time (min)	Deg. (%)	Ref.
Cu	Co-precipitation	MB	60	63	[23]
Cu	Hydrothermal	MB	120	65	[24]
Au	Surfactant free phytochemical reduction	MB	180	76	[25]
Mn	Ion-exchange method	MB	240	90	[26]
Ag	Electrochemical method	MB	120	52	This work

The photocatalytic activity of the ZnO may decrease due to higher surface doping, which covers the surface of ZnO and prevents light and pollutant adsorption. Table 1 shows Ag, Cu, Au and Mn transition metals effect on the photodegradation of MB dye. In comparison with previous reported works containing transition elements doped ZnO photocatalysts, Ag-doped ZnO photocatalyst in this study had a comparable photocatalytic activity under UV light. According to Table 1, Ag-doped ZnO nanorods may be appropriate for wastewater treatment.

The degradation rates of MB dye was based on the Langmuir–Hinshelwood model. According to this model, the rate constants for degradation (k) were determined by the linear fit taken from the -lnC/C0 versus time data (Fig. 5). All samples were studied under the same conditions for 120 min. As shown in Fig. 5, the magnitude of k exhibits the following ordering; Ag doped-ZnO/PSi > ZnO/PSi >pure PSi. These results indicate that the Ag doping enhances the photocatalytic activity as seen from the results. The improvement is due to the enhancement of photogenerated electron-hole pairs as a result of varied potential energy between ZnO and Ag.

To test the effect of Ag-doped ZnO/PSi photocatalyst in MB removal from real water subjected to MB contamination, tap-water and dye wastewater were used as the matrices of the adsorption solution, and the results are indicated in Table 2. It was observed that the removal efficiency for MB in wastewater was higher than that in tap-water when initial MB concentration is 200 mg/L. Mainly, in wastewater with 200 mg/L MB, the removal efficiency of Ag-doped ZnO/PSi was 94.86%. This high MB removal efficiency of Ag-doped ZnO/PSi in wastewater may result from a higher pH, and it indicates the great application potential of Ag-doped ZnO/PSi in removing MB from wastewater.

Table 2. Efficiency of MB removal by Ag-doped ZnO/PSi from real water samples after 12 h contact time in room temperature

Real samples	pH	Initial concentration of MB	Residual concentration of MB	Removal efficiency (%)
Tap-water	7.1	200 mg/L	14.34 mg/L	92.83
Wastewater	8.3	200 mg/L	10.28 mg/L	94.86

4. CONCLUSION

Vertically aligned Ag doped-ZnO NRs were successfully synthesized on seed-layer-free PSi structures using an electrochemical technique. FESEM results indicated that c-axis orientation was the preferential growth direction of the single-crystalline Ag doped-ZnO NRs, consistent with XRD results. The EIS was applied to analyze interface properties and charge transfer efficiency of samples. The removal of methylene blue as an organic compound in wastewater using the Ag doped-ZnO/PSi photoanodes was studied by the photoelectrocatalytic technique. The EIS results show that Ag doped-ZnO/PSi nanostructures have higher free-electron carriers which accelerate charge transfer and decrease the resistance. About 41% of MB was removed in 120 min when the ZnO/PSi photoelectrode was applied for the photoelectrocatalytic process, while it enhanced to 52% when using the Ag doped-ZnO/PSi electrode. The enhanced photocatalytic activity of the Ag doped-ZnO/PSi can be attributed to the enhancement of photogenerated electron-hole pairs as a result of varied potential energy between ZnO and Ag.

ACKNOWLEDGMENTS
This work is supported by National Natural Science Foundation of China Youth Science Foundation Project (Project No. C161203), the World-Class Discipline Construction and Characteristic Development Guidance Funds for Beijing Forestry University 2019XKJS0320.

References

1. S. Xia, Z. Song, P. Jeyakumar, S.M. Shaheen, J. Rinklebe, Y.S. Ok, N. Bolan and H. Wang, *Critical reviews in environmental science and technology*, 49 (2019) 1027.
2. S.S. Ray, S.-S. Chen, C.-W. Li, N.C. Nguyen and H.T. Nguyen, *RSC Advances*, 6 (2016) 85495.
3. M.C. Chrispim, M. Scholz and M.A. Nolasco, *Journal of environmental management*, 248 (2019) 109268.
4. B.C. Hodges, E.L. Cates and J.-H. Kim, *Nature nanotechnology*, 13 (2018) 642.
5. G. Darabdhara, P.K. Boruah, P. Borthakur, N. Hussain, M.R. Das, T. Ahamad, S.M. Alshehri, V. Malgras, K.C.-W. Wu and Y. Yamauchi, *Nanoscale*, 8 (2016) 8276.
6. A. Alhadhrami, A.S. Almalki, A.M.A. Adam and M.S. Refat, *International Journal of Electrochemical Science*, 13 (2018) 6503.
7. H.-C. Hsu, C.-S. Cheng, C.-C. Chang, S. Yang, C.-S. Chang and W.-F. Hsieh, *Nanotechnology*, 16 (2005)
8. J. Rouhi, C.R. Ooi, S. Mahmud and M.R. Mahmood, *Mater Lett*, 147 (2015) 34.
9. X. Sheng, T. Xu and X. Feng, *Advanced Materials*, 31 (2019) 1805132.
10. T. Munawar, F. Iqbal, S. Yasmeen, K. Mahmood and A. Hussain, *Ceramics International*, 46 (2020) 2421.
11. L.-l. Wang, W. Ma, J.-l. Ma and G.-q. Shao, *International Journal of Electrochemical Science*, 14 (2019) 9150.
12. V. Mote, Y. Purushotham and B. Dole, *Materials & Design*, 96 (2016) 99.
13. Ş.Ş. Türkyılmaz, N. Güy and M. Özacar, *Journal of Photochemistry and Photobiology A: Chemistry*, 341 (2017) 39.

14. A. Alhadhrami, A.S. Almalki, A.M.A. Adam and M.S. Refat, *International Journal of electrochemical Science*, 13 (2018) 6503.
15. C. Chen and Y. Chen, *Appl Phys Lett*, 75 (1999) 2560.
16. M. Alimanesh, J. Rouhi and Z. Hassan, *Ceram Int*, 42 (2016) 5136.
17. S.A. Ansari, M.M. Khan, S. Kalathil, A. Nisar, J. Lee and M.H. Cho, *Nanoscale*, 5 (2013) 9238.
18. K.L. Foo, U. Hashim, K. Muhammad and C.H. Voon, *Nanoscale Res Lett*, 9 (2014) 429.
19. M. Husairi, J. Rouhi, K. Alvin, Z. Atikah, M. Rusop and S. Abdullah, *Semiconductor Science and Technology*, 29 (2014) 075015.
20. H. Karimi-Maleh, C.T. Fakude, N. Mabuba, G.M. Peleyeju and O.A. Arotiba, *Journal of colloid and interface science*, 554 (2019) 603.
21. Y.-M. Lee, C.-M. Huang, H.-W. Chen and H.-W. Yang, *Sens Actuators A Phys*, 189 (2013) 307.
22. M.E. Fragalà, A. Di Mauro, D.A. Cristaldi, M. Cantarella, G. Impellizzeri and V. Privitera, *Journal of Photochemistry and Photobiology A: Chemistry*, 332 (2017) 497.
23. N. Prasad, V. Saipavitra, H. Swaminathan, P. Thangaraj, M.R. Viswanathan and K. Balasubramanian, *Applied Physics A*, 122 (2016) 590.
24. S.-H. Hsieh and J.-M. Ting, *Applied Surface Science*, 427 (2018) 465.
25. M.K. Choudhary, J. Kataria and S. Sharma, *ACS Applied Nano Materials*, 1 (2018) 1870.
26. Q. Ma, X. Lv, Y. Wang and J. Chen, *Optical Materials*, 60 (2016) 86.